ISSN 1063-7397, Russian Microelectronics, 2016, Vol. 45, Nos. 8–9, pp. 625–632. © Pleiades Publishing, Ltd., 2016.
Original Russian Text © D.A. Agarkov, M.A. Borik, S.I. Bredikhin, V.T. Bublik, L.D. Iskhakova, A.V. Kulebyakin, I.E. Kuritsyna, E.E. Lomonova, F.O. Milovich, V.A. Myzina, S.V. Seryakov, N.Yu. Tabachkova, 2015, published in Izvestiya Vysshikh Uchebnykh Zavedenii, Materialy Elektronnoi Tekhniki, 2015, Vol. 18, No. 4, pp. 246–254.

Influence of the Yttria Dopant on the Structure and Properties of $(ZrO_2)_{0.91-x}(Sc_2O_3)_{0.09}(Y_2O_3)_x$ ($x = 0$–0.02) Crystals

D. A. Agarkov[a], M. A. Borik[b], S. I. Bredikhin[a], V. T. Bublik[c], L. D. Iskhakova[b, d], A. V. Kulebyakin[b], I. E. Kuritsyna[a], E. E. Lomonova[a], F. O. Milovich[b], V. A. Myzina[a], S. V. Seryakov[b, c], and N. Yu. Tabachkova[b, *]

[a] *Institute of Solid State Physics, Russian Academy of Sciences, ul. Akademika Osip'yana 2, Chernogolovka, Moscow oblast, 142432 Russia*

[b] *Prokhorov Institute of General Physics, Russian Academy of Sciences, ul. Vavilova 38, Moscow, 119991 Russia*

[c] *National Research University of Science and Technology MISIS, Leninskii pr. 4, Moscow, 119049 Russia*

[d] *Research Center of Fiber Optics, Russian Academy of Sciences, ul. Vavilova 38, Moscow, 119991 Russia*

**e-mail: ntabachkova@gmail.com*

Received April 4, 2016

Abstract—We have studied the influence of the yttrium oxide (Y_2O_3) dopant (1 and 2 mol %) on the phase composition, structure, and electrical properties of ZrO_2–9 mol % Sc_2O_3 solid solution. Stabilization of ZrO_2 jointly with 9 mol % Sc_2O_3 and 2 mol % Y_2O_3 is shown to allow the acquisition of high phase stability transparent homogeneous crystals with a cubic structure. Their mechanical grinding is established to cause no change in the phase composition of these crystals, whereas the powders retain the initial fluorine structure. The powders preserved the original structure of the fluorite crystals. All the probed crystals reveal high microhardness and low fracture toughness. Increasing the Y_2O_3 concentration in the crystals led to a reduction of the maximum loads on the indenter, which the sample withstood without cracking. As is shown, the specific conductivity exhibits nonmonotonic behavior depending on the Y_2O_3 concentration in the crystals. Increasing the Y_2O_3 content to 2 mol % in the solid electrolyte reduces the conductivity of the crystals in the entire temperature range that is attributed to a decrease in the carrier mobility due to the increasing ion radius of the stabilizing ion.

Keywords: solid electrolytes, zirconia, crystal growth, single crystals, phase transitions, twins, ionic conductivity, mechanical properties

DOI: 10.1134/S1063739716080023

INTRODUCTION

The application of stabilizing scandium oxide in solid electrolytes based on zirconium dioxide allows one to obtain material with high ionic conductivity. The electrolytic membranes made of this composite favor a significant decrease in the working temperature of the electrochemical device while retaining high conductivity. It is important for improving the operational resource and reliability of the electrochemical reactors, solid-oxide fuel elements, electrolyzers, and sensors [1–5].

According to various references [6–10], ZrO_2–(9–10) mol % Sc_2O_3 ceramic possesses the highest ionic conductivity. However, many works [6–11] report the high sensitivity of this ceramic to Sc_2O_3. As is mentioned in [11], ceramic with 9.3 mol % Sc_2O_3 shows the highest ionic conductivity. Besides the cubic phase, there is the formation of a rhombohedral phase with the Sc_2O_3 increasing concentration to 9.5 mol % in the ceramic at room temperature. Compared to the cubic phase, the rhombohedral phase possesses weak conductivity. Upon heating, the rhombohedral phase passes to the cubic phase at temperatures of 400 to 600°C. During the stabilization of the boundaries of zirconia oxide with scandium oxide, the existence of phases are determined only approximately. This is caused by the metastable phases in this system and, consequently, by the dependence of the phase composition on the technique and conditions of the synthesis of the material. As was shown in [1, 2], the additional doping of ZrO_2–Sc_2O_3 systems with yttrium and cerium oxides allows the acquisition of more stable highly conductive cubic solid solutions.

Unlike ceramics, the synthesis of single crystal materials enables one to exclude the effect of factors such as the grain sizes, the distribution of the solid solution component through the bulk and boundaries of the grains, intergrain stress, and the alteration of these parameters under high temperatures close to the

Table 1. Compositions, designations, and appearance of $(ZrO_2)_{0.91-x}(Sc_2O_3)_{0.09}(Y_2O_3)_x$ ($x = 0$–0.02) crystals

Sample	Composition, mol %			Appearance
	ZrO_2	Sc_2O_3	Y_2O_3	
9ScSZ	91	9	0	Completely muddy crack-free crystal
9Sc1YSZ	90	9	1	Alternated transparent and muddy domains in crystal
9Sc2YSZ	89	9	2	Completely transparent homogeneous single crystals

working temperatures of solid-oxide fuel elements on the electrophysical characteristics of the material.

This work is aimed at estimating the influence of 1 and 2 mol % Y_2O_3 dopant oxide on the phase composition, structure, and electrophysical properties of ZrO_2–9 mol % Sc_2O_3.

EXPERIMENTAL

The solid solution single crystals were grown via directed melt crystallization in a cold container with a diameter of 130 mm on a Cristall-407 setup at a growth rate of 10 mm/h. The weight of the deposited material was 4–5 kg, and the rate of crystallization was 10 mm/h. The cooling rate of the crystallized melt ingot on the melt temperature (~3000°C) to 1000°C ranged from 180 to 2000°C/min, and then from 180 to 250°C/min to room temperature. The Y_2O_3 content in the initial charge was varied from 0 to 2 mol % at the constant Sc_2O_3 concentration of 9 mol %. The charge was prepared from the zirconium and scandium oxide powders with the preoursor content of 99.99%.

The ($10 \times 10 \times 2$ mm^3) samples were cut from the crack-free crystals. The chemical composition of the crystals was probed via X-ray spectroscopy on a JEOL 5910 LV scanning electron microscope. The phase composition of the samples was controlled via Raman spectroscopy on a Renishaw inVia system and via X-ray diffraction on a Bruker D8 diffractometer under CuK_α radiation. The crystal structure was studied on a JEM 2100 transmission electron microscope at an accelerating voltage of 200 kV. The sample was thinned via ion etching on a PIPS II setup. High-temperature Raman spectra were obtained on a laboratory setup equipped with a high-temperature atmospheric furnace, an Avesta-Proekt optical scheme (Russia), a MDR-6 diffraction monochromator (Lomo Ltd., Russia), and a CCD camera (Princeton Instruments, USA) [12]. The density was determined via hydrostatic weighing on a Sartorius system (the measurement error was 0.05%). The microhardness of the crystals was measured on a DM 8B AUTO microhardometer at the loads of 100–300 g. The transport characteristics of the crystals were studied over the temperature range of 450–900°C with the increment of 50°C on a Solartron SI 1260 analyzer at the frequencies of 1 Hz to 5 MHz. The measurements were implemented on 7×7 mm^2 slices with a thickness of 0.5 mm and symmetrical platinum electrodes. For this the bars were covered with a platinum paste and were then annealed at 950°C for 1 hour in air. The amplitude of the applied AC signal was 24 mV. The frequency impedance spectrum was carefully analyzed in the ZView software. The resistances of the electrolytes were calculated from the obtained impedance spectra followed by the evaluation of the specific electric conductivity of crystals.

RESULTS AND DISCUSSION

ZrO_2 crystals stabilized with 9 mol % Sc_2O_3 and doped with 1 and 2 mol % Y_2O_3 were grown via directed melt crystallization in a cool container. The acquired crystals are described in Table 1. The cross sections of the crystals were of 10 to 15 mm and the length of the crystal varied from 30 to 45 mm. The 9ScSZ crystals were transparent and revealed no cracks there (Fig. 1a). Embedding 1 mol % Y_2O_3 caused the emergence of transparent domains in the crystals (Fig. 1b). The transparent areas were found in the bottom part of the crystals that corresponded to the onset of crystallization, whereas the semitransparent zones were in the upper part of the crystals (the end of crystallization). In some crystals the transparent and semi-transparent areas alternated in the central part of the crystallized melt ingot (Fig. 1b). An increase in the Y_2O_3 content to 2 mol % resulted in the acquisition of transparent homogeneous single crystals (Fig. 1c).

Figure 2 displays the composition of the 9ScSZ crystals which is shown with an arrow in the ZrO_2–Sc_2O_3 phase diagram [13, 14]. There are various options of ZrO_2–Sc_2O_3 state diagrams, which differ from each other, especially in the ZrO_2–9 mol % Sc_2O_3 area. The equilibrium phase composition at temperatures below 1000°C was not reliably established. According to the state diagrams, the cubic (c) phase upon cooling can undergo transformation into a tetragonal (t), rhombohedral (r), or even monoclinic phase [15]. There are no data on the tricomponent ZrO_2–Sc_2O_3–Y_2O_3 system reported in the literature.

The analysis of the Sc_2O_3 and Y_2O_3 distribution through the crystal length revealed that all the studied samples are homogeneous in their composition and the Sc_2O_3 and Y_2O_3 concentrations are in agreement

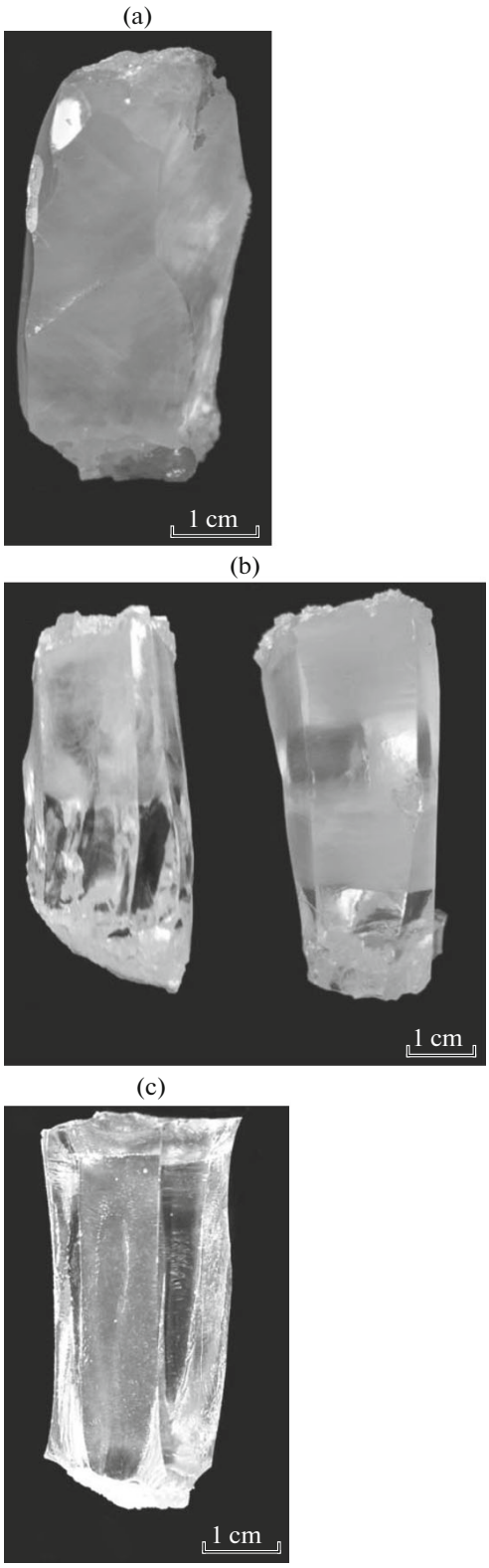

Fig. 1. (a) 9ScSZ, (b) 9Sc1YSZ and (c) 9Sc2YSZ crystals.

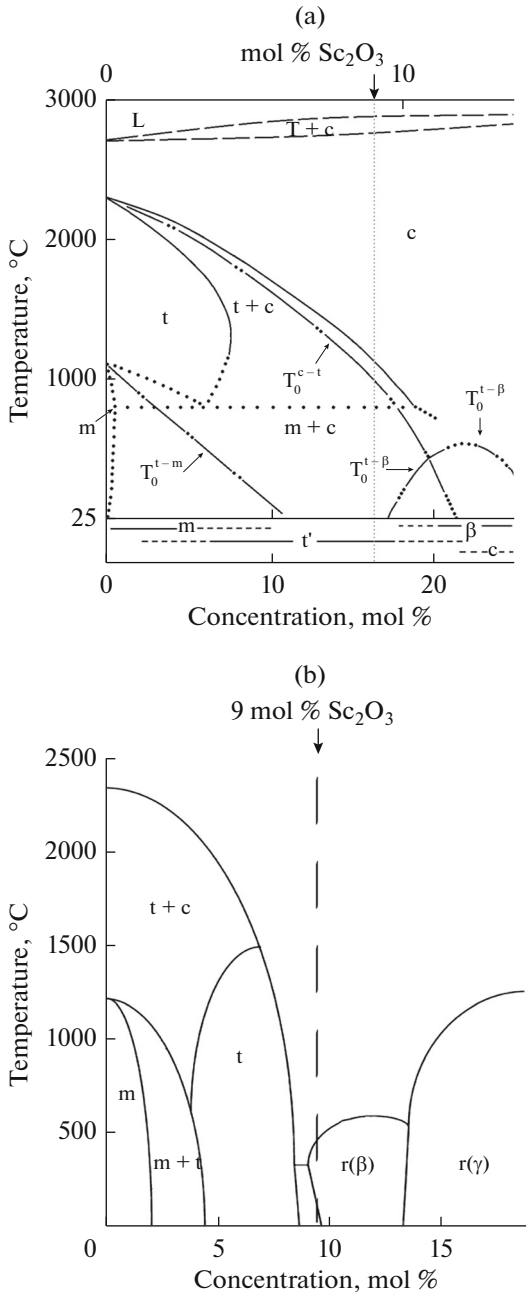

Fig. 2. ZrO_2–Sc_2O_3 state diagrams: (a) [13]; (b) [14].

with their content in the initial charge. The samples exhibit a weak trend to the decreasing Sc_2O_3 content through the crystal length that means the effective Sc_2O_3 content distribution coefficient is slightly superior to 1. Figure 3 shows the Sc_2O_3 and Y_2O_3 distribution in the 9Sc1YSZ crystal.

The Sc_2O_3 and Y_2O_3 concentrations were measured near the boundary with the semitransparent and transparent zones in the 9Sc1YSZ crystals at several points (Table 2). The difference between the Y_2O_3 concentrations in the semitransparent and transparent areas of the crystal is extremely low and close to 1 mol %. As is seen from Table 2, the increasing Sc_2O_3 and Y_2O_3 concentrations allow one to achieve the transparent

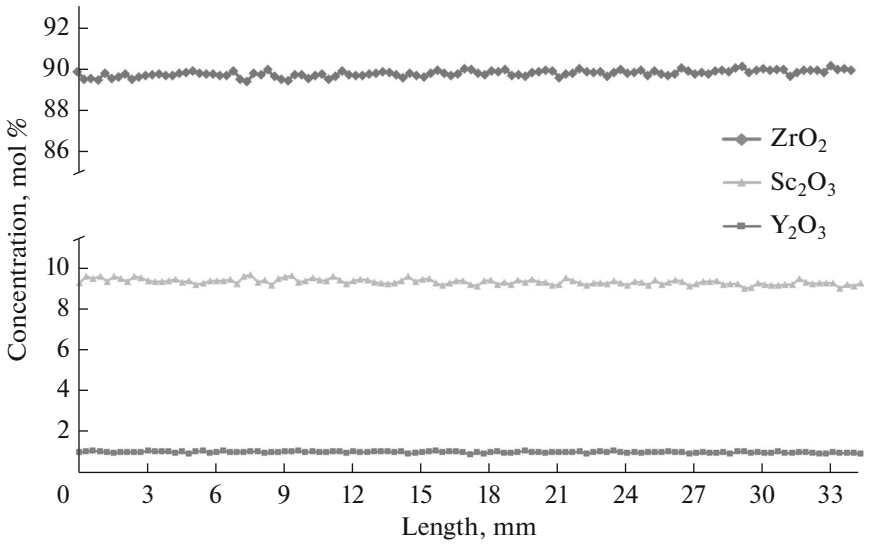

Fig. 3. Scandium and yttrium oxide distributions over the length in 9Sc1YSZ crystals.

homogeneous crystals that correspond to the appearance and Sc_2O_3 and Y_2O_3 concentrations within the crystal length. A decrease in the concentration at the end of the melt crystallization (Fig. 3) of a sample slightly depleted with Sc_2O_3 and Y_2O_3 dopants leads to the formation of a semitransparent area in the upper part of the crystal (Fig. 1b). The quasi-equivalent Sc_2O_3 and Y_2O_3 concentrations in the transparent and semitransparent zones of the 9Sc1YSZ crystal may cause their interleaving through the crystal length (Fig. 1b). This effect was observed in crystals from the central part of the crystallized melt ingot. The variations in the dopant oxide concentrations in this part of the ingot can be more pronounced because of the lower axis temperature gradients. This is typical of zirconia-based crystals grown via directed crystallization in a cool container [16].

The phase composition of crystals and powders was probed via X-ray diffraction (Table 3). The powders were characterized in order to evaluate the phase stability of the crystals to the mechanical exposure.

As is obvious from Table 3, 9ScSZ crystals do not undergo phase transition upon attrition. This means that the transformation hardening mechanism cannot be implemented in 9ScSZ crystals, when the moving microcrack induces the martensitic tetragonal–monoclinic transition which absorbs the stress energy and blocks the moving crack, unlike ZrO_2 crystals partially stabilized with Y_2O_3 [17]. The systems with zirconia exhibit the low diffusive coefficients of ions at temperatures below 1400°C [18]. The existence of only a tetragonal phase in 9ScSZ crystals is caused by the fact that the cubic-to-biphase area transition temperature is 1000°C (Fig. 2a) [13] or even lower [14] (Fig. 2b). This favors the quenching of the cubic phase below 1400°C, which passes into the tetragonal phase with the parameters close to the cubic phase without undergoing the phase alteration upon cooling.

Table 2. Composition of transparent and semitransparent domains in 9Sc1YSZ crystals

Appearance	Concentration, mol %	
	Sc_2O_3	Y_2O_3
Muddy area	8.38 ± 0.13	0.71 ± 0.20
Transparent area	8.86 ± 0.14	1.08 ± 0.19

The ZrO_2 crystals stabilized with 9 mol % Sc_2O_3 and additionally doped with Y_2O_3 reveal the emergence of a cubic phase. In the semitransparent areas of 9Sc1YSZ crystals, the cubic phase coexists with the tetragonal phase, while the transparent zones of the crystals are single-phase with a cubic structure. However, the cubic phase in these areas is unstable and partially passes into the tetragonal phase upon abrasion. In 9Sc2YSZ crystals there is only a cubic ZrO_2 modification, and no phase transition was observed in these crystals upon abrasion.

The phase composition of the crystals was also studied via Raman spectroscopy (Fig. 4). Besides the lines from the tetragonal phase, there is the presence of a band at 366 cm^{-1} in the Raman spectrum of the 9ScSZ crystal. In [19] this line is assigned to the oxygen defects in ZrO_2–Sc_2O_3 tetragonal solid solutions. Nevertheless, the emergence of an additional line can also be due to the rhombohedral phase inclusions in these crystals.

In 9Sc2YSZ crystals the peak positions match those typical of a cubic phase. The Raman spectra of 9Sc1YSZ crystals reveal the presence of tetragonal and cubic phases.

Table 3. Phase composition of $(ZrO_2)_{0.91-x}(Sc_2O_3)_{0.09}(Y_2O_3)_x$ ($x = 0$–0.02) solid solution crystals and powders

Sample	Appearance	Phase composition	
		crystals	powders
9ScSZ	Semi-transparent	t	t
9Sc1YSZ	Semi-transparent	c + t	c + t
	Transparent	c	
9Sc2YSZ	Transparent	c	c

c—cubic ZrO_2; t—tetragonal ZrO_2.

The phase transition temperatures in the 9ScSZ and 9Sc1YSZ crystals were determined via high-temperature Raman spectroscopy. The spectra were recorded in the temperature range of 20–900°C with an increment of 100°C (Fig. 5). For 9ScSZ crystals (Fig 6a) with increasing temperature, all spectral lines were continuously shifted with no pronounced changes in the spectra up to 700°C. The tetragonal phase lines decrease at the temperatures of 700–900°C, and the tetragonal lines 326 and 475 cm^{-1} vanish at 900°C. In 9Sc1YSZ crystals a decreasing band intensity from the tetragonal phase was observed at 600°C (Fig. 6b). Thus, in 9Sc1YSZ crystals composed of the tetragonal phase and part of the cubic phase, the tetragonal-to-cubic phase transition starts at a temperature of 600°C. It is 100°C lower than the onset temperature of the transition in 9ScSZ crystals.

Table 4 shows the data on the density and mechanical characteristics of the crystals. The density of the crystals decreases with the increasing Y_2O_3 concentration, which is due to the impact of Y_2O_3 with the specific weight superior to Sc_2O_3, as well as the phase composition of the crystals, on the density of the studied crystals. Despite the embedding of the heavier Y_2O_3 in the tetragonal 9ScSZ crystal, the density of the crystal is reduced because of the combination of the tetragonal and cubic phases in 9Sc1YSZ, while the 9Sc2YSZ crystal is completely cubic. All the studied crystals possess high microhardness and low crack resistance. The increasing Y_2O_3 concentration in the crystals causes the need to diminish the maximum loads on the indenter, which are withstood by the sample without the emergence of cracks. The microhardness was measured at the loads whose values are shown in Table 4.

The TEM studies reveal the presence of twins in 9Sc1YSZ crystals. As is seen in Fig. 6a, the primary twin plates of a crystal are in turn counterpart. The traces of secondary twinning planes are at an angle of ~60° relative to the trace of the primary twinning. The formation of twins upon the cubic-to-tetragonal transition in 9ScSZ crystals is analogous to the formation of the twin structure in ZrO_2–Y_2O_3 crystals [17]. It is worth mentioning that the presence of twins favors the improvement of the mechanical characteristics in the material and causes no cracking in the crystals during the phase transition. While measuring the microhardness (Table 4), the 9ScSZ crystals withstand severe

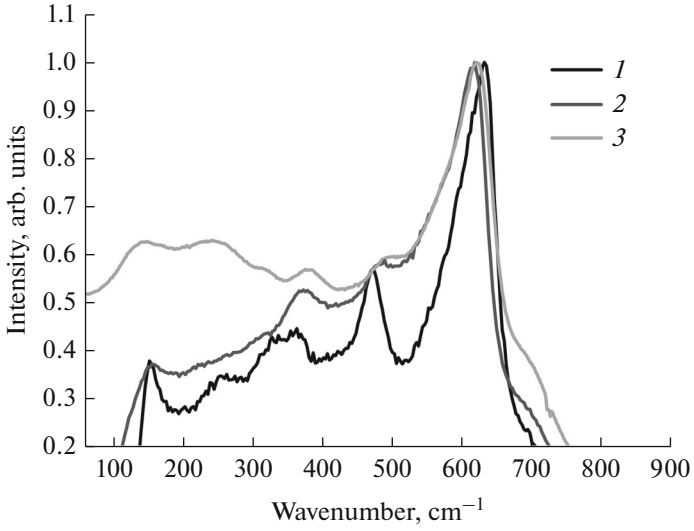

Fig. 4. Raman spectra of: *1*—9ScSZ; *2*—9Sc2YSZ; *3*—9Sc1YSZ crystals.

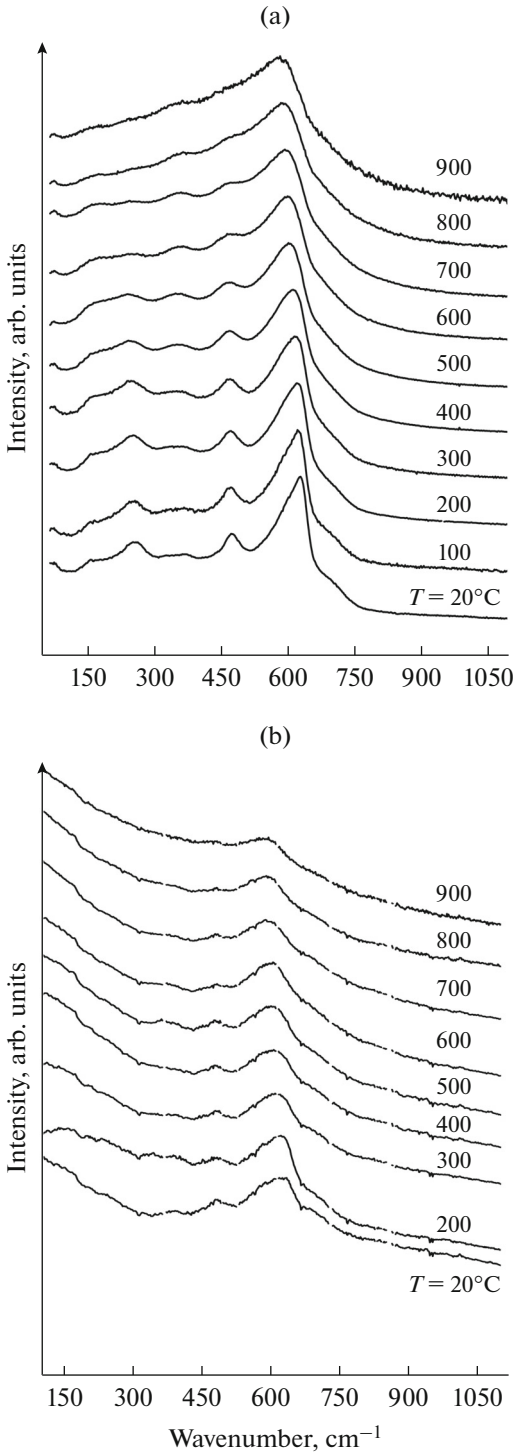

Fig. 5. Raman spectra of the studied crystals over the temperature range of 20 to 900°C: (a) 9ScSZ; (b) 9Sc1YSZ.

loads in the indentation without cracking compared to the cubic crystals. Nevertheless, the lack of a transformation hardening mechanism substantially reduces the crack resistance in crystals in comparison to the partially stabilized ZrO_2–Y_2O_3 crystals [17].

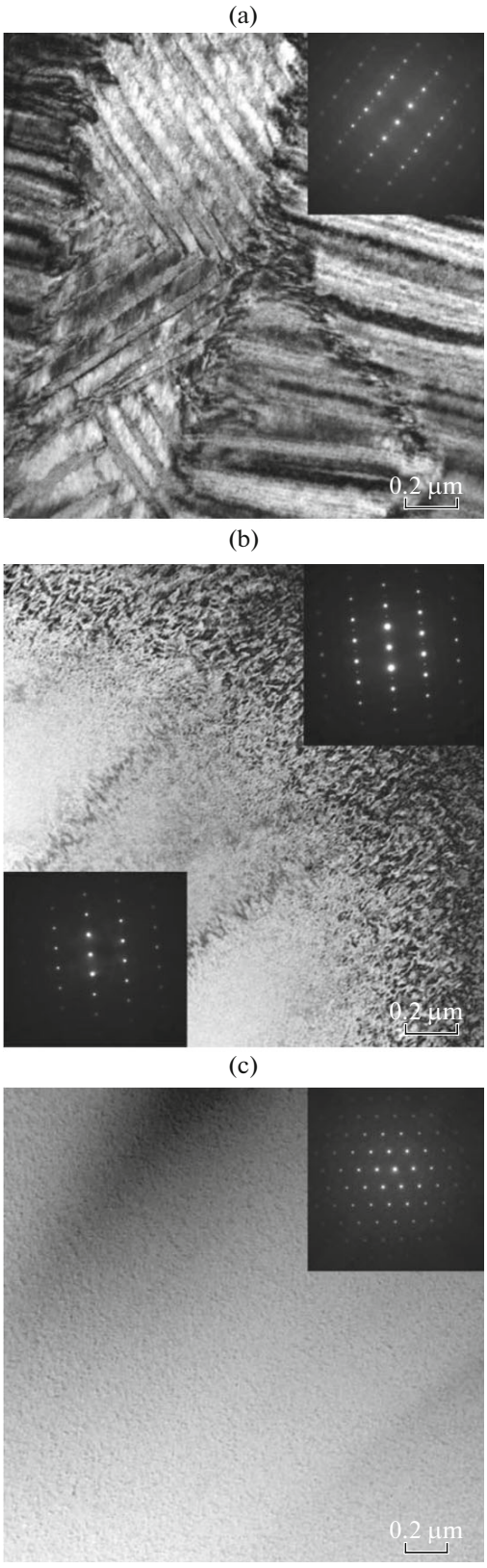

Fig. 6. TEM image of crystals: (a) 9ScSZ, insert—diffraction pattern of t-ZrO_2; (b) 9Sc1YSZ, insert—diffraction pattern of c-ZrO_2 (in the bottom), t-ZrO_2 (at the top); (c) 9Sc2YSZ, insert—diffraction pattern of c-ZrO_2.

Table 4. Density and mechanical characteristics of $(ZrO_2)_{0.91-x}(Sc_2O_3)_{0.09}(Y_2O_3)_x$ ($x = 0$–0.02) crystals

Sample	Appearance	Density, g/cm^3	Microhardness HV, kgf/mm^2	Load, N
9ScSZ	Semi-transparent	5.807 ± 0.001	1590 ± 20	2.0
9Sc1YSZ	Semi-transparent	5.788 ± 0.005	1610 ± 20	1.5
	Transparent	5.769 ± 0.005	1715 ± 20	1.0
9Sc2YSZ	Transparent	5.760 ± 0.001	1650 ± 20	0.5

Table 5. Activation energy and specific conductivity of $(ZrO_2)_{0.91-x}(Sc_2O_3)_{0.09}(Y_2O_3)_x$ ($x = 0$–0.02) solid solution crystals over the temperature range of 973–1173 K

Sample	E_a, eV		$E_a = E_{as} + E_m$		Specific conductivity, Ω^{-1} cm^{-1}			
	673–823 K	823–1173 K	E_{as}	E_m	973 K	1073 K	1123 K	1173 K
9ScSZ	1.36	0.79	0.57	0.79	0.024	0.054	0.075	0.097
9Sc1YSZ	1.33	0.63	0.70	0.63	0.033	0.063	0.077	0.094
9Sc2YSZ	1.37	0.77	0.60	0.77	0.019	0.043	0.057	0.072

Figure 6b displays the image of the interface between the cubic and tetragonal phases in the 9Sc1YSZ crystal. The tetragonal phase twins in this crystal are ultrafine and homogeneous in size. The appearance and size of the twins in the tetragonal 9ScSZ crystal and in crystals composed of the cubic and tetragonal phases are different by the lack of twins in cubic 9Sc2YSZ crystals (Fig. 6c).

Figure 7 shows the temperature dependences of specific conductivity in the studied crystals plotted in the Arrhenius coordinates. Obviously, the conductivity of the 9Sc1YSZ crystals is superior to that of the 9ScSZ crystals in the whole temperature range. As follows from the phase composition study, the post-growth 9Sc1YSZ crystals are composed of a cubic phase, in addition to the tetragonal phase, which defines their higher conductivity at temperatures up to 900°C compared to the tetragonal 9ScSZ crystals. At a temperature of 900°C both 9ScSZ and 9Sc1YSZ crystals become completely cubic, and the conductivity values for these compositions are almost equal. Embedding 2 mol % Y_2O_3 in the solid electrolyte causes a decrease in the conductivity. Among the studied solid electrolytes, 9Sc2YSZ crystals exhibit the lower conductivity values in the whole temperature range. According to the data in Table 5 for the 9Sc1YSZ crystals, the activation energy at high temperatures is inferior to that for the 9Sc2YSZ crystals. The mobility of the carriers thus decreases with the rising Y_2O_3 concentration. Moreover, the association energy diminishes from 0.70 to 0.60 eV with the increasing Y_2O_3 concentration, which coincides with the results acquired on ceramics in [20], where the conductivity was shown to decrease, while increasing the Y_2O_3 concentration. This was attributed to the reduced carrier mobility because of the ionic radius enlargement in the stabilizing oxide.

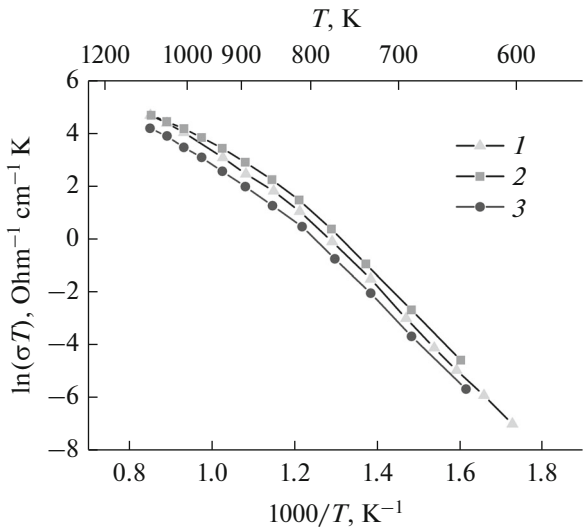

Fig. 7. Temperature dependences of conductivity in crystals: *1*—9ScSZ; *2*—9Sc2YSZ; *3*—9Sc1YSZ.

CONCLUSIONS

$(ZrO_2)_{0.91-x}(Sc_2O_3)_{0.09}(Y_2O_3)_x$ ($x = 0$–0.02) solid solution crystals were for the first time grown via the oriented crystallization. Stabilization with 9 mol % Sc_2O_3 and 2 mol % Y_2O_3 was shown for the acquisition of transparent homogeneous crystals with a cubic structure. The analysis of the yttrium and scandium oxide distribution through the crystal length revealed the homogeneity of the composition of the studied

crystals, and the Sc_2O_3 and Y_2O_3 concentrations were almost equal to those in the pristine charge. The phase analysis of the 9Sc2YSZ crystals and powders revealed their high phase stability, because the mechanical grinding caused no change in the phase composition of these crystals. For bi-phase 9Sc1YSZ crystals, the tetragonal-to-cubic phase transition was found to start at 600°C, which was 100°C below the onset temperature of the transition in the single-phase tetragonal 9ScSZ crystal. Increasing the Y_2O_3 concentration to 2 mol % in the solid electrolyte caused a decrease in the conductivity of the 9Sc2YSZ crystals compared to the 9Sc1YSZ crystals in the whole temperature range, which was attributed to a decrease in the carrier mobility due to the increasing radius of the stabilizing ion.

ACKNOWLEDGMENTS

This work was supported by the Russian Foundation for Basic Research (projects ofi_m nos. 14-29-04081 and 13-03-12408).

REFERENCES

1. Badwal, S.P.S., Ciacchi, F.T., and Milosevic, D., Scandia-zirconia electrolytes for intermediate temperature solid oxide fuel cell operation, *Solid State Ionics,* 2000, vols. 136–137, nos. 1–2, pp. 91–99. doi 10.1016/S0167-2738(00)00356-8
2. Kharton, V.V., Marques, F.M.B., and Atkinson, A., Transport properties of solid oxide electrolyte ceramics: a brief review, *Solid State Ionics,* 2004, vol. 174, nos. 1–4, pp. 135–149. doi 10.1016/j.ssi.2004.06.015
3. Fergus, J.W., Electrolytes for solid oxide fuel cells, *J. Power Sources,* 2006, vol. 162, no. 1, pp. 30–40. doi 10.1016/j.jpowsour.2006.06.062
4. Yokokawa, H., Sakai, N., Horita, T., Yamaji, K., and Brito, M.E., Solid oxide electrolytes for high temperature fuel cells, *Electrochemistry,* 2005, vol. 73, no. 1, pp. 20–30.
5. Politova, T.I. and Irvine, J.T.S., Investigation of scandia-yttria-zirconia system as an electrolyte material for intermediate temperature fuel cells–influence of yttria content in system $(Y_2O_3)_x(Sc_2O_3)_{(11-x)}(ZrO_2)_{89}$, *Solid State Ionics,* 2004, vol. 168, nos. 1–2, pp. 153–165. doi 10.1016/j.ssi.2004.02.007
6. Wakako, A., Hanashiro, D., Arai, Y., and Malzbender, J., Fracture mechanism of scandia-doped zirconia, *Acta Mater.,* 2013, vol. 61, no. 8, pp. 3082–3089. doi 10.1016/j.actamat.2013.01.068
7. Fujimori, H., Yashima, M., Kakihana, M., and Yoshimura, M., Structural changes of scandia-doped zirconia solid solutions: rietveld analysis and saman scattering, *J. Am. Ceram. Soc.,* 1998, vol. 81, no. 11, pp. 2285–2293. doi 10.1111/j.1151-2916.1998.tb02710.x
8. Simoncic, P. and Navrotsky, A., Systematics of phase transition and mixing energetics in rare earth, *J. Am. Ceram. Soc.,* 2007, vol. 90, no. 7, pp. 2143–2150. doi 10.1111/j.1551-2916.2007.01678.x
9. Spirin, A., Ivanov, V., Nikonov, A., Lipilin, A., Paranin, S., Khrustov, V., and Spirina, A., Scandia-stabilized zirconia doped with yttria: synthesis, properties, and ageing behavior, *Solid State Ionics,* 2012, vol. 225, pp. 448–452. doi 10.1016/j.ssi.2012.02.022
10. Tataryn, T., Savytskii, D., Paulmann, C., and Bismayer, U., Twin structure of the ZrO_2–Sc_2O_3 crystal, *Cryst. Rad. Phys. Chem.,* 2009, vol. 78, no. 10, pp. 101–104. doi 10.1016/j.radphyschem.2009.03.088
11. Shobit, O., Najib, W.B., Chen, W., and Bonanos, N., Electrical conductivity of 10 mol % Sc_2O_3–1 mol % M_2O_3–ZrO_2 ceramics, *J. Am. Ceram. Soc.,* 2012, vol. 95, no. 6, pp. 1965–1972. doi 10.1111/j.1551-2916.2012.05126.x
12. Agarkov, D.A., Burmistrov, I.N., Tsybrov, F.M., Tartakovskii, I.I., Kharton, V.V., Bredikhin, S.I., and Kveder, V.V., Analysis of interfacial processes at the SOFC electrodes by in-situ Raman spectroscopy, *ECS Trans.,* 2015, vol. 68, no. 1, pp. 2093–2103. doi 10.1149/06801.2093ecst
13. Yashima, M., Kakihana, M., and Yoshimura, M., Metastable-stable phase diagrams in the zirconia-containing systems utilized in solid-oxide fuel cell application, *Solid State Ionics,* 1996, vols. 86–88, no. 2, pp. 1131–1149. doi 10.1016/0167-2738(96)00386-4
14. Chiba, R., Yoshimura, F., Yamaki, J., Ishii, T., Yonezawa, T., and Endou, K., Ionic conductivity and morphology in Sc_2O_3 and Al_2O_3 doped ZrO_2 films prepared by the sol-gel method, *Solid State Ionics,* 1997, vol. 104, nos. 3–4, pp. 259–266. doi 10.1016/S0167-2738(97)00423-2
15. Sheu, T.-S., Xu, J., and Tien, T.-Y., Phase relationships in the ZrO_2–Sc_2O_3 and ZrO_2–In_2O_3 Systems, *J. Am. Ceram. Soc.,* 1993, vol. 76, no. 8, pp. 2027–2032. doi 10.1111/j.1151-2916.1993.tb08328.x
16. Kuzminov, Yu.S., Lomonova, E.E., and Osiko, V.V., *Tugoplavkie materialy iz kholodnogo tilgya* (Refractory Materials from Cold Crucible), Moscow: Nauka, 2004.
17. Borik, M.A., Bublik, V.T., Kulebyakin, A.V., Lomonova, E.E., Milovich, F.O., Myzina, V.A., Osiko, V.V., and Tabachkova, N.Y., Phase composition, structure and mechanical properties of PSZ (partially stabilized zirconia) crystals as a function of stabilizing impurity content, *J. Alloys Compd.,* 2014, vol. 586, pp. 231–235. doi 10.1016/j.jallcom.2013.01.126
18. Andrievskaya, E.R., *Fazovye ravnovesiya v sistemakh oksidov gafniya, tsirkoniya, ittriya s oksidami redkozemel'nykh elementov* (Phase Equilibrium in Hafnium, Zirconium, Yttrium Oxyde Systems with Rare Earth Element Oxydes), Kiev: Naukova Dumka, 2010.
19. Fujimori, H., Yashima, M., Kakihana, M., and Yoshimura, M., β-Cubic phase transition of scandia-doped zirconia solid solution: calorimetry, X-ray diffraction, and Raman scattering, *J. Appl. Phys.,* 2002, vol. 91, no. 10, pp. 6493–6498. doi 10.1063/1.1471576
20. Arachi, Y., Sakai, H., Yamamoto, O., Takeda, Y., and Imanishai, N., Electrical conductivity of the ZrO–Ln_2O_3 (Ln = lanthanides) system, *Solid State Ionics,* 1999, vol. 121, nos. 1–4, pp. 133–139. doi 10.1016/S0167-2738(98)00540-2

Translated by O. Maslova